




Acoustic impurity shielding induced by a pair of metasurfaces respecting \mathcal{PT} symmetryHaixiao Zhang ^{1,2,*}, Yiwei Zhang,³ Xiaoli Liu,¹ Yu Bao ¹ and Jinyu Zhao ^{4,†}¹*School of Electrical and Information Engineering, Changzhou Institute of Technology, Changzhou 213032, China*²*MOE Key Laboratory of Modern Acoustics, Nanjing University, Nanjing 210093, China*³*School of Aviation and Mechanical Engineering, Changzhou Institute of Technology, Changzhou 213032, China*⁴*Key Laboratory of Architectural Acoustic Environment of Anhui Higher Education Institutes, Anhui Jianzhu University, Hefei 230601, China*

(Received 2 June 2022; revised 25 August 2022; accepted 29 August 2022; published 13 September 2022)

Impurities usually affect the transmission of acoustic signals, and how to effectively suppress their adverse effects is an important content in the research of acoustic materials. In a recent theoretical proposal, it was pointed out that perfect transmission through impurities can be achieved by adding a gain-loss distribution respecting parity-time (\mathcal{PT}) symmetry. In this paper, we demonstrate a similar but not identical way to realize the extraordinary physical property of impurity-shielding, which leads to perfect transmission at the so-called exceptional points. By systematically probing into the system composed of an equivalent medium slab sandwiched by a pair of \mathcal{PT} -symmetric metasurfaces, we obtain the two complementary solutions of exceptional points corresponding to perfect transmission. Interestingly, the two solutions of exceptional points coalesce into one when the mass density of the slab approaches zero. At such a critical point, we find that the impurity-shielding effect can be perfectly demonstrated, irrespective of embedded impurities of almost any shape and materials, whether they are Hermitian or non-Hermitian. In addition, the proposed system is frequency independent, indicating that the prototype can work well even in the subwavelength range. Our paper shows that exceptional points can be used to eliminate scattering of impurities in a density-near-zero medium, revealing their potential applications in acoustic sensing, directional imaging, and other related wave disciplines.

DOI: [10.1103/PhysRevB.106.094101](https://doi.org/10.1103/PhysRevB.106.094101)**I. INTRODUCTION**

Sound wave is one of the important methods of communication in people's daily life, however, it is easily reflected by obstacles and form complex interference patterns [1]. Suppressing any such distortions of a wave's free propagation is an challenging task for many active research areas [2–4], such as biomedical imaging [2], acoustic cloaking [3], and metamaterial design [4]. Considerable efforts have been devoted to predict the modified properties of acoustic media embedded with impurities in difference scenarios [5–7]. In recent years, a seemingly unrelated concept, topological insulators, has been introduced into the field of acoustics, facilitating an approach to realize impurity-shielding for surface waves, which are robust against impurities and defects on the surface [8–13]. Similarly, tremendous effort has been devoted in the surface waves of topological insulators as well as their electromagnetic analog [14–17]. However, the nature of topological insulators only supports edge states instead of bulk states on a very narrow band. To the best of our knowledge, the extraordinary property of acoustic impurity-shielding for bulk states has not been realized yet.

Another potential approach to achieve perfect transmission of a system is to imprint on it a suitable distribution of gain and loss in the context of non-Hermitian wave

physics, a research area initially driven by theoretical and experimental studies of non-Hermitian systems that respect parity-time (\mathcal{PT}) symmetry [18–36]. The gain and loss in the materials allow the deviation from a conventional Hermitian system and introduce additional physics based on \mathcal{PT} -phase transition and the associated exceptional points (EPs). Many intriguing acoustic phenomena and applications have been predicted and observed, such as acoustic cloaks [20], invisible sensors [21,22], flexible control of EPs [23], unidirectional transparency [24], tunability of piezoelectric semiconductors [25,26], periodic \mathcal{PT} -symmetric structures [27], total transmission band [28], discrete [29], and step-wise [30] constant-pressure waves. More recently, the concept of \mathcal{PT} symmetry has been introduced into acoustic metasurfaces, which renders many exciting novel phenomena such as acoustic metasurface cloak [37] and negative refraction [38]. However, only free space was considered between the \mathcal{PT} -symmetric metasurfaces, making their physical mechanisms no different from those of the previous bulk \mathcal{PT} -symmetric materials, in particular the propagation mechanisms of sound waves between the metasurfaces.

In this paper, we theoretically demonstrate a principle to realize impurity-shielding for acoustic waves, which leads to perfect transmission irrespective of embedded impurities of almost any materials. The extraordinary property is induced by the introduction of a pair of \mathcal{PT} -symmetric metasurfaces that sandwich a slab of equivalent medium. Two complementary types of EPs have been observed, at one of which the metasurfaces function as a pair of coherent perfect absorber

* zhanghx@nju.edu.cn

† jyzhao@ahjzu.edu.cn

(CPA) and laser, which has been mentioned in previous report [21]. The other very different type of EP is rarely mentioned, at which the metasurfaces function as a pair of unidirectional antireflection coatings (ARCs) for general media or metamaterials. If the equivalent medium is replaced to the density-near-zero (DNZ) medium, we can compensate for the divergent impedance contrast between the DNZ media and free space with well designed \mathcal{PT} -symmetric metasurfaces. More importantly and interestingly, by utilizing the \mathcal{PT} -symmetric metasurfaces, we find that the initial doping effect of impurities in DNZ media is significantly suppressed, thus achieving perfect transmission of the impurity-shielding effect. In addition, the system is frequency independent, indicating that the prototype works well even in the subwavelength range. Our paper shows that exceptional points can be used to eliminate scattering of impurities in a DNZ medium, revealing their potential applications in acoustic sensing, directional imaging, and in other related wave disciplines.

II. RESULTS AND DISCUSSION

A. Accessing exceptional points of any sandwiched slab

We begin with a pair of lossy (left) and gain (right) metasurfaces separated by a slab with relative mass density ρ and relative bulk modulus κ , as illustrated in Fig. 1(a). When the surface impedances of the metasurfaces are opposite to each other with $\pm|Z_s|$, the acoustic \mathcal{PT} -symmetric condition is satisfied. In such a \mathcal{PT} -symmetric system, the scattering matrix describing the relation between the incoming and outgoing waves can be written as

$$S = \begin{bmatrix} t & r_R \\ r_L & t \end{bmatrix}, \quad (1)$$

where $r_{L(R)}$ is the reflection coefficient for left (right) incidence, and t is the transmission coefficient for both incidences since the system is reciprocal. Under the \mathcal{PT} -symmetric nature of the acoustic system with $S^* = S^{-1}$, we can obtain the generalized energy-conservation relation [20]

$$\sqrt{R_L R_R} = |T - 1|, \quad (2)$$

where $R_{L(R)} \equiv |r_{L(R)}|^2$ and $T \equiv |t|^2$, are the reflectance and transmittance for left (right) incidence, respectively.

From Eq. (1), the eigenvalues of the scattering matrix are expressed as $\lambda_{1,2} = t \pm \sqrt{r_L r_R}$. Using Eq. (2), we further have $\lambda_{1,2} = t[1 \pm i\sqrt{(1-T)/T}]$. From this relation, we can conclude that when $T < 1$ ($T > 1$), eigenvalues are unimodular (nonunimodular), and the acoustic system is in the so-called symmetric (broken) phase. The transition between these two phases happens at the EPs and we have $T = 1$, and $R_L R_R = 0$, indicating unity transmission and R_L and/or R_R is zero. As a result, at the EPs, acoustic \mathcal{PT} -symmetric systems can exhibit the so-called unidirectional transparency.

To achieve $T = 1$, the impedances of the metasurfaces at the EPs should satisfy (see Supplemental Material [39])

$$Z_s = (1 \pm \sqrt{\rho\kappa})Z_0, \quad (3)$$

for normal incidence. Here, the “ \pm ” sign indicates that there exist two solutions of EPs, and they are complementary to each other but have very different physical nature as we shall see later. More clearly, the transmission coefficient of the

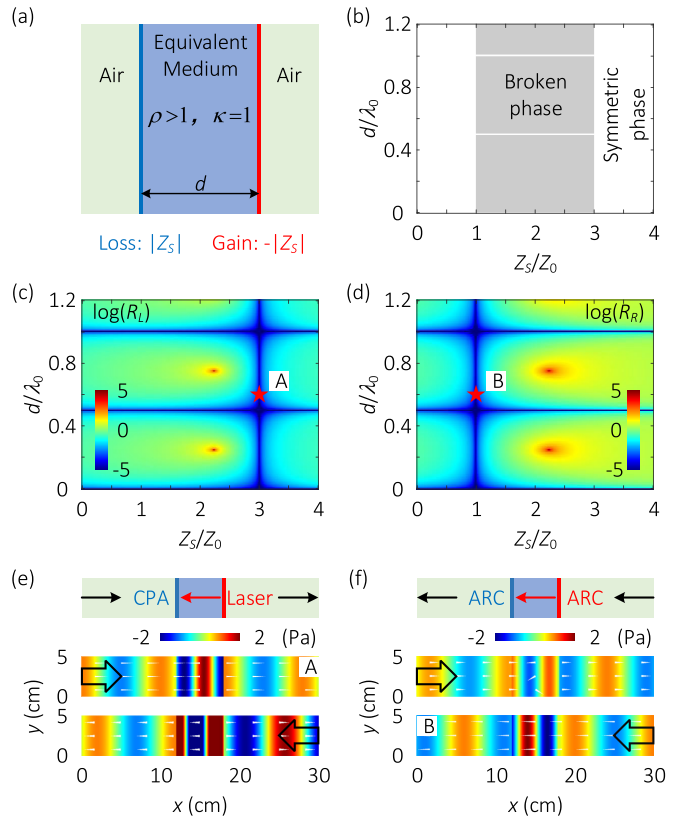


FIG. 1. (a) Illustration of the \mathcal{PT} -symmetric system composed of a slab with relative mass density ρ and relative bulk modulus κ sandwiched by a pair of \mathcal{PT} -symmetric metasurfaces with impedances $\pm|Z_s|$. (b) Phase diagram for normal incidence. [(c),(d)] Reflectance for left (c) and right (d) incidence as functions of d/λ_0 and Z_s/Z_0 on the \mathcal{PT} -symmetric system. The red pentagrams marked as “A” and “B” are the EPs of the scattering matrix of the \mathcal{PT} -symmetric system. [(e),(f)] Illustration of the CPA-laser (ARC-ARC) mode at the EP of “A” (“B”) and the associated simulated pressure distributions with $d = 0.6\lambda_0$. The surface impedance at “A” and “B” are $Z_s = 3Z_0$ and $Z_s = -Z_0$, respectively. The time-averaged power flow has been shown by white tapers for each model. In panels (b)–(f), the parameters of the slab are $\rho = 4$ and $\kappa = 1$.

system in both solutions can be expressed as

$$t = e^{\pm i\alpha}, \quad (4)$$

where $\alpha = kd = \sqrt{\rho\kappa}^{-1}k_0d$, and k (k_0) is the wave number in the slab (air). We stipulate that, when $Z_s > 0$ ($Z_s < 0$), the solution gives $R_L = 0$ ($R_R = 0$) for incidence on the lossy (gain) metasurface. Interestingly, both solutions of $T = 1$ are independent of the thickness d of the sandwiched slab, but not for the transmission t , as predicted in the theory. Moreover, the influence of the thickness of the metasurfaces on the full transmission can be effectively suppressed by appropriate experimental methods.

For convenience, we set $\kappa = 1$ in this paper without affecting the expected results. The phase diagram for normal incidence is shown in Fig. 1(b), with relative mass density $\rho = 4$. The white and gray regions denote the symmetric and broken phases, respectively, while EPs are between the \mathcal{PT} -symmetric and broken phases with $Z_s = 3Z_0$ and $Z_s = -Z_0$,

both independent of d . The two values are consistent with the plus and minus signs in Eq. (3), respectively. Incidentally, the region of broken phase has a width of $2Z_0$ and is symmetrically distributed around the center of $Z_s = \sqrt{\rho}Z_0$. We emphasize that the additional white lines (at $d = j/2\lambda_0$, and j is an integer) in the broken region are induced by Fabry-Perot resonances of the slab, independent of Z_s . Ulteriorly, we plot the reflectance for left and right incidence as functions of d/λ_0 and Z_s/Z_0 on the \mathcal{PT} -symmetric system in Figs. 1(c) and 1(d), respectively. As expected, we can find left-side unidirectional transparency [vertical blue line in (c)] with $R_L = 0$, $T = 1$ at $Z_s = 3Z_0$ and right-side unidirectional transparency [vertical blue line in (d)] with $R_R = 0$, $T = 1$ at $Z_s = -Z_0$. The horizontal blue lines in (c) and (d) indicate that there is no reflection for either left or right incidence, corresponding to the white lines in Fig. 1(b).

In order to further understand the different physical mechanisms of the two series of EPs, we select two points in (c) and (d) with $d = 0.6\lambda_0$, marked as ‘‘A’’ and ‘‘B’’, respectively. The field distribution obtained by using COMSOL multiphysics at EP ‘‘A’’ with $Z_s = 3Z_0$ and $R_L = 0$ is shown in Fig. 1(e). Here, the frequency of the incident wave is $f = 3.43$ kHz. The energy flux flows from the right to the left inside the slab, indicating that the lossy metasurface absorbs the impinging energy from both sides, while the gain metasurface radiates toward both sides. In this sense, the functionality of \mathcal{PT} -symmetric metasurfaces is a pair of CPA and Laser, denoted as a CPA-laser pair. In addition, the transmission coefficient in this case can be derived as $t = e^{i2k_0d}$ [Eq. (4)], featuring the anomalous phase advance at the transmission side.

On the other hand, we demonstrate the field distribution at EP ‘‘B’’ with $Z_s = -Z_0$ and $R_R = 0$ at the same frequency, as shown in Fig. 1(f). In this case, the energy flux flows from the right to the left inside the slab, which is the same as those in free space. Therefore, the functionality of \mathcal{PT} -symmetric metasurfaces is a pair of ARCs, denoted as an ARC-ARC pair instead of a CPA-Laser pair. In contrast to the transmission coefficient at EP ‘‘A’’, we have $t = e^{-i2k_0d}$ [Eq. (4)] in this case, featuring the anomalous phase lag at the transmission side.

A notable point is that the EPs associated with the ARC-ARC pair have not been reported in acoustics before, because only free space was considered between the \mathcal{PT} -symmetric metasurfaces previously, in which such EPs do not exist. Here, with both types of complementary EPs given by a unified formula of Eq. (3), the solutions of the EPs are complete. Another point worth noting is that when the relative density of the slab changes from $\rho > 1$ to $\rho < 1$, an interesting transition behavior appears for the EPs associated with an ARC-ARC pair of metasurfaces. The details have been discussed in the Supplemental Material [39], in which the region of broken phase has a width of $2\sqrt{\rho}Z_0$ and is symmetrically distributed around the center of $Z_s = Z_0$. By the way, we mark two associated EPs as ‘‘C’’ and ‘‘D’’ in this case.

B. Accessing exceptional points of DNZ medium slab

Next, we consider the idiosyncratic case of a DNZ medium slab with $\rho = 10^{-4}$ between the \mathcal{PT} -symmetric metasurfaces, as shown in Fig. 2(a). Similarly, the phase diagram for normal

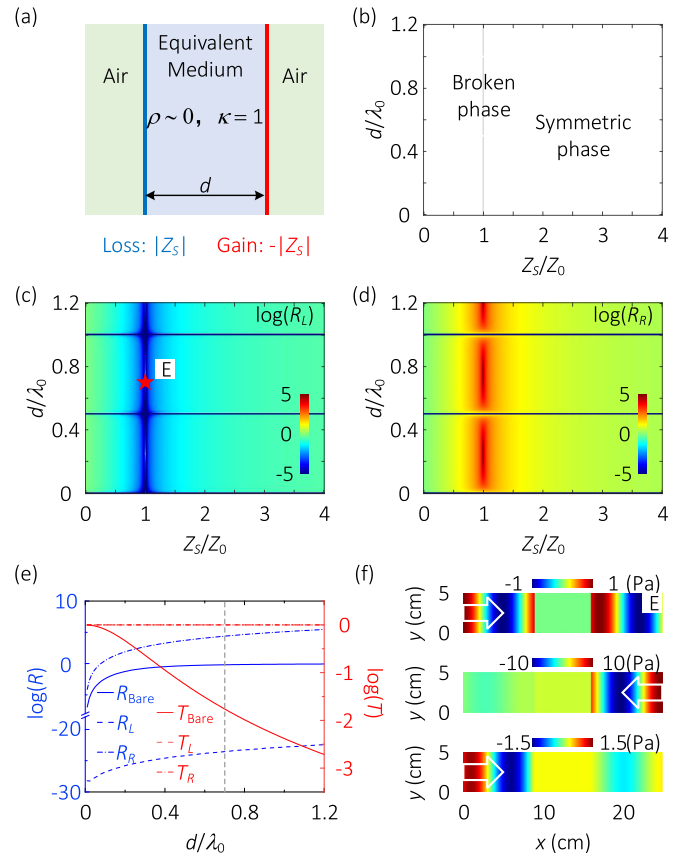


FIG. 2. (a) Illustration of the \mathcal{PT} -symmetric system. (b) Phase diagram for normal incidence with $\rho = 10^{-4}$ and $\kappa = 1$. [(c),(d)] Reflectance for left (c) and right (d) incidence as functions of d/λ_0 and Z_s/Z_0 on the \mathcal{PT} -symmetric system. The red pentagram marked as ‘‘E’’ is the EP of the scattering matrix of the \mathcal{PT} -symmetric system. (e) Reflectance and transmittance for DNZ medium with and without \mathcal{PT} -symmetric metasurfaces by varying d/λ_0 . (f) Distribution of pressure in and out of the slab for the case with \mathcal{PT} -symmetric metasurfaces ($Z_s = 1.01Z_0$) for left incidence (top), right incidence (middle), and the case without \mathcal{PT} -symmetric metasurfaces (bottom) at $d = 0.7\lambda_0$ [gray-vertical line in (e)].

incidence is plotted in Fig. 2(b). An interesting and inevitable phenomenon is that the region width of the \mathcal{PT} -broken phase $2\sqrt{\rho}Z_0$ will shrink to 0 significantly, resulting to the corresponding two EPs converge to the same value of $Z_s = Z_0$. In other words, the two original solutions of EPs coalesce into one EP when $\rho \rightarrow 0$. We redraw the R_L and R_R of the system in Figs. 2(c) and 2(d), and the unidirectional transparency is observed only from the left side, but not from the right side, corresponding to the discussion in the Supplemental Material [39]. An EP marked as ‘‘E’’ with $d = 0.7\lambda_0$ and $Z_s = 1.01Z_0$ in (c) has been chosen to prepare for further clarification.

Figure 2(e) illustrates how the \mathcal{PT} -symmetric metasurfaces tune the scattering behavior of the system from total reflection to robust perfect transmission at ‘‘E’’, overcoming the impedance mismatch between DNZ medium and air. The solid blue and red curves represent the reflectance and transmittance for DNZ medium without \mathcal{PT} -symmetric metasurfaces by varying d/λ_0 . It can be seen that for very small d , the tiny transmission still exists, while with d increasing,

we observe almost total reflectance ($R_{\text{Bare}} = 1$) and near-zero transmission ($T_{\text{Bare}} \rightarrow 0$) due to the divergent impedance mismatch. For comparison, when the \mathcal{PT} -symmetric metasurfaces are applied, near-zero reflectance from left side ($R_L \rightarrow 0$, blue dashed curve), and unity transmittance ($T = T_L = T_R = 1$, red-dashed and dash-dotted curves) are observed, irrespective of d . Not surprisingly, we can find the reflectance from the right side $R_R \neq 0$, indicating that the perfect transmission is unidirectional. Besides, R_R is a function of d , which enables the system to carry out other engineering applications under the premise of maintaining left-side transparency. The above results are discussed on the basis of $Z_s = 1.01Z_0$ associated with “E” for the CPA-Laser pair. In fact, such a phenomenon can also be realized by using the EP for the ARC-ARC pair, at which the surface impedance is $Z_s = 0.99Z_0$.

In Fig. 2(f), we simulate the distribution of pressure for the aforementioned three cases at $d = 0.7\lambda_0$, associated with the gray vertical line in Fig. 2(e). For the case of equipped \mathcal{PT} -symmetric metasurfaces ($Z_s = 1.01Z_0$) for left incidence (top panel), the expected perfect transmittance with $R_L = 0$ and $T = 1$ is observed. Interestingly, if we look more closely at the distribution, we can find that the transmission coefficient is almost 1 without any phase advance or lag, as if the DNZ material did not exist. This phenomenon can usually not be obtained in a single \mathcal{PT} -symmetric structure, except by periodic structure [40] or other methods. Here, we can derive this result straightway according to Eq. (4), in which $\alpha = \sqrt{\rho}k_0d \rightarrow 0$, thus we obtain $\text{Arg}(t) = \alpha \rightarrow 0$. As for the case of right incidence (middle panel), the wave is transmitted to left side with same amplitude of one and phase of zero, consistent with reciprocity, but an additional strong reflection arises at this side, associated with a large standing wave ratio. For comparison, in bottom panel, we show that removal of the \mathcal{PT} -symmetric metasurfaces leads to very low transmission, due to the divergent impedance mismatch between the DNZ medium and air (see the Supplemental Material [39]).

C. Impurity shielding effect and its physical mechanism

In the following, we will demonstrate how DNZ material can combine with \mathcal{PT} -symmetric metasurfaces to obtain impurity-shielding effect and explain its physical mechanism by applying field analysis. In preparation, we investigate the case of placing a circular impurity with radius R_c and relative density $\rho_c = 4$ in middle of DNZ material in the model of Fig. 2(a), and the simulated transmittance can be seen in Fig. 3(a). Clearly, without the \mathcal{PT} -symmetric metasurfaces (dashed curves), T varies dramatically as R_c/λ_0 increases, and almost has nothing to do with the exact density ($\rho = 10^{-2}$, 10^{-4} and 10^{-6}) of the DNZ material. Apparently, a very small region around a singular point at $R_c = 0.192\lambda_0$ is caused by the Fabry-Perot resonance of the system, and has a significant influence on the impurity-shielding effect. It means that when the \mathcal{PT} -symmetric metasurfaces are applied, the sound waves will still be partly reflected at the singular point if ρ is not small enough ($\rho = 10^{-2}$ and 10^{-4} , green and red solid curves). However, when the DNZ medium approaches an ideal value, the transmittance $T \rightarrow 1$, even near the singular point of $R_c = 0.192\lambda_0$ ($\rho = 10^{-6}$, blue solid curve).

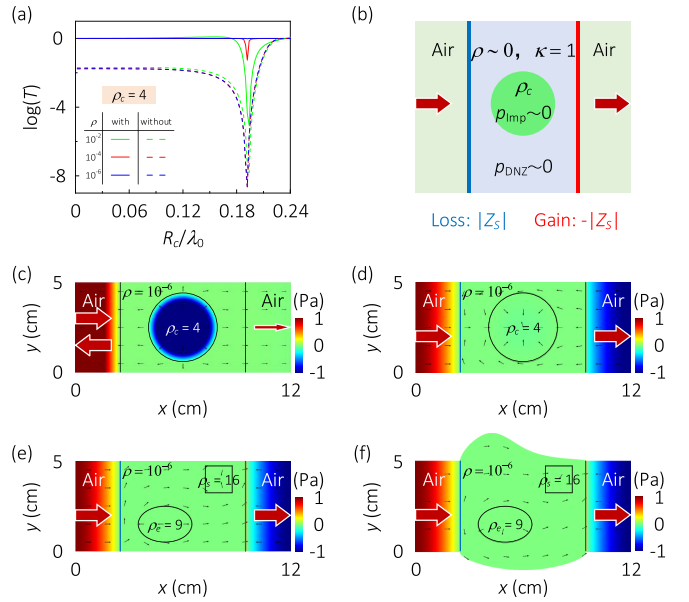


FIG. 3. (a) Transmittance as a function of R_c/λ_0 for the case of the DNZ medium with (solid curves) and without (dashed curves) the \mathcal{PT} -symmetric metasurfaces. (b) Schematic of the pressure field analysis for the impurity-shielding model with \mathcal{PT} -symmetric metasurfaces. [(c),(d)] Distributions of pressure for the doping model and the impurity-shielding model, respectively. A circular impurity of $\rho_c = 4$ exists in both cases. [(e),(f)] Distribution of pressure for the impurity-shielding model with arbitrary impurities and general geometrical configurations, respectively. A elliptic impurity of $\rho_e = 9$, and a square impurity of $\rho_s = 16$ exist in both cases. In panels (c)–(f), the width of the DNZ medium slab is $d = 0.7\lambda_0$, and the black arrows show the direction and amplitude of the air velocity.

Our previous discussion is focused on the scattering matrix of the \mathcal{PT} -symmetric system rather than the pressure field inside the slab. In the Supplemental Material [39] we derive the pressure distribution inside and outside the slab with the existence of the \mathcal{PT} -symmetric metasurfaces, where there is only one unidirectional plane wave inside the slab, and its pressure amplitude can be expressed as $p = (Z/Z_0)p_i = \sqrt{\rho}p_i$. Here, p_i is the amplitude of the incident wave. Peculiarly, when the DNZ medium is applied ($\rho \rightarrow 0$), the pressure inside the slab $p_{\text{DNZ}} \sim 0$. In this situation, any impurity put into DNZ material will not affect the pressure inside the slab ($p_{\text{Imp}} \sim 0$), thus obtaining the impurity-shielding effect, as shown in Fig. 3(b).

We deliberately choose the singular point of $R_c = 0.192\lambda_0$ to prove the effectiveness of the device. Figures 3(c) and 3(d) illustrate the pressure distribution of the system without and with the \mathcal{PT} -symmetric metasurfaces, respectively, naming doping model and impurity-shielding model. Obviously, in doping model, sound waves barely pass through the system, and the sound energy is confined to the circular impurity. While in the impurity-shielding model, we obtain perfect transmission, with a nonexistent sound field inside the circular impurity, showing the strong ability of \mathcal{PT} -symmetric super-surfaces to suppress doping effect. This phenomenon can be extended to more general situations, as shown in Figs. 3(e) and 3(f), in which we exhibit the distribution of pressure for the impurity-shielding model with arbitrary impurities (a elliptic

impurity of $\rho_e = 9$, and a square impurity of $\rho_s = 16$) and general geometrical configurations, respectively. As expected, the pressure in DNZ medium and impurities is 0, and the system achieves perfect transmission.

The introduction of non-Hermitian media can significantly change the impurity-shielding effect of the system. In the Supplemental Material [39] we analyze in great detail the influences of the non-Hermitian materials on the impurity-shielding effects, including the non-Hermitian slab, non-Hermitian DNZ media and non-Hermitian impurities. The simulation results indicate that the impurity-shielding phenomenon is widely enslaved to non-Hermitian slab; slightly affected by absolute value of relative density of the non-Hermitian DNZ medium, and almost irrespective of the non-Hermitian property of the impurities.

Distinct from the non-Hermitian media, the frequency of the incident waves has a highly limited influence on the \mathcal{PT} -symmetric system, as presented in the Supplemental Material [39]. We simulate three models in Fig. 1, Fig. 2, and Fig. S5(d) (see the Supplemental Material [39]), respectively, on both CPA-Laser and ARC-ARC pairs of the system. The impurity-shielding effect remains robust in all cases, however the impedances of metasurfaces also need to be adjusted considering the dispersion of slab when it is a real geometry except for a DNZ medium.

III. SUMMARY

To summarize, we derive the scattering EPs of a equivalent medium slab sandwiched by a pair of \mathcal{PT} -symmetric metasurfaces in acoustics. A rarely reported type of EP at which the metasurfaces function as a pair of ARCs is revealed, and the direction of its transmission resonance depends on the impedance ratio of the slab to air. When the slab morphs into a DNZ medium, the original two EPs approach each other to the coalescence point of $Z_s = Z_0$. Interestingly, at the critical point of $\rho \rightarrow 0$, not only can the significant problem of huge impedance mismatch with free space be solved, but also the doping effect of DNZ media can be

significantly suppressed, resulting in unprecedented acoustic impurity-shielding properties of bulk waves. The physical mechanism of impurity-shielding is that the acoustic pressure is close to zero in the boundary region of DNZ medium. Therefore, the principle can be applied to impurities of almost any shape and materials, whether they are Hermitian or non-Hermitian.

In practical realization, both types of metasurfaces in the \mathcal{PT} -symmetric system can be realized by designing suitable circuits due to the emergence of the active acoustic metamaterials [13,21]. At the same time, acoustic DNZ media can be demonstrated at certain frequencies of phononic crystals [41]. These works manifest the possibility of realizing the metasurfaces with the required effective parameters. Our method can be applied to different fields such as electronics, optics, microwaves and elastic metamaterials. Especially in recent years, preliminary studies have been made on \mathcal{PT} symmetry in elastic wave system [42–44]. In view of the correlation between elastic and sound waves, elastic metamaterials may also provide potential ideas for experimental realization of acoustic \mathcal{PT} symmetry, and vice versa. This design ability over the \mathcal{PT} -symmetric system opens an avenue for developing asymmetric wave transport devices, which can be applied as directional imaging, sensing, logic devices in any complex operating environments.

ACKNOWLEDGMENTS

This work was supported by the National Natural Science Foundation of China (Grant No. 11904035), the Program for High-Level Entrepreneurial and Innovative Talents Introduction of Jiangsu Province, Changzhou Sci&Tech Program (Grant No. CJ20200040) and the Natural Science Foundation of the Jiangsu Higher Education Institutions of China (Grant No. 20KJB510028). J.Z. acknowledges the support from the Anhui Provincial Natural Science Foundation (Grant No. 1908085QA39) and from the major Scientific Research Projects in Colleges and Universities of Educational Commission of Anhui Province (Grant No. KJ2019A0780).

-
- [1] V. Twersky, *J. Acoust. Soc. Am.* **53**, 96 (1973).
 - [2] K. M. Mudry, R. Plonsey, and J. D. Bronzino, *Biomedical Imaging* (CRC Press, Boca Raton, FL, 2003).
 - [3] S. A. Cummer and D. Schurig, *New J. Phys.* **9**, 45 (2007).
 - [4] S. A. Cummer, J. Christensen, and A. Alù, *Nat. Rev. Mater.* **1**, 16001 (2016).
 - [5] S. Mizuno and S.-i. Tamura, *Phys. Rev. B* **45**, 13423 (1992).
 - [6] E. H. El Boudouti, B. Djafari-Rouhani, A. Akjouj, and L. Dobrzynski, *Surf. Sci. Rep.* **64**, 471 (2009).
 - [7] Z. Wang, H. Yang, D. Zhao, R. Wang, and G. Jin, *AIP Adv.* **9**, 105205 (2019).
 - [8] Z. Yang, F. Gao, X. Shi, X. Lin, Z. Gao, Y. Chong, and B. Zhang, *Phys. Rev. Lett.* **114**, 114301 (2015).
 - [9] C. He, X. Ni, H. Ge, X. Sun, Y. Chen, M. Lu, X. Liu, and Y. Chen, *Nat. Phys.* **12**, 1124 (2016).
 - [10] X. Ni, M. A. Gorlach, A. Alu, and A. B. Khanikaev, *New J. Phys.* **19**, 055002 (2017).
 - [11] H. Dai, J. Jiao, B. Xia, T. Liu, S. Zheng, and D. Yu, *J. Phys. D: Appl. Phys.* **51**, 175302 (2018).
 - [12] S. Huo, J. Chen, L. Feng, and H. Huang, *J. Acoust. Soc. Am.* **146**, 729 (2019).
 - [13] B. Hu, Z. Zhang, H. Zhang, L. Zheng, W. Xiong, Z. Yue, X. Wang, J. Xu, Y. Cheng, X. Liu, and J. Christensen, *Nature (London)* **597**, 655 (2021).
 - [14] S. Girvin and R. Prange, *The Quantum Hall Effect* (Springer, New York, 1987).
 - [15] F. D. M. Haldane and S. Raghu, *Phys. Rev. Lett.* **100**, 013904 (2008).
 - [16] Z. Wang, Y. D. Chong, J. D. Joannopoulos, and M. Soljačić, *Phys. Rev. Lett.* **100**, 013905 (2008).
 - [17] Z. Wang, Y. Chong, J. D. Joannopoulos, and M. Soljačić, *Nature (London)* **461**, 772 (2009).
 - [18] C. M. Bender and S. Boettcher, *Phys. Rev. Lett.* **80**, 5243 (1998).

- [19] C. M. Bender, S. Boettcher, and P. N. Meisinger, *J. Math. Phys.* **40**, 2201 (1999).
- [20] X. Zhu, H. Ramezani, C. Shi, J. Zhu, and X. Zhang, *Phys. Rev. X* **4**, 031042 (2014).
- [21] R. Fleury, D. L. Sounas, and A. Alù, *Nat. Commun.* **6**, 5905 (2015).
- [22] R. Fleury, D. L. Sounas, and A. Alù, *IEEE J. Sel. Top. Quant.* **22**, 121 (2016).
- [23] C. Shi, M. Dubois, Y. Chen, L. Cheng, H. Ramezani, Y. Wang, and X. Zhang, *Nat. Commun.* **7**, 11110 (2016).
- [24] Y. Aurégan and V. Pagneux, *Phys. Rev. Lett.* **118**, 174301 (2017).
- [25] J. Christensen, M. Willatzen, V. R. Velasco, and M. H. Lu, *Phys. Rev. Lett.* **116**, 207601 (2016).
- [26] Z. Hou and B. Assouar, *J. Appl. Phys.* **123**, 085101 (2018).
- [27] W. Ji, Q. Wei, X. Zhu, D. Wu, and X. Liu, *Europhys. Lett.* **125**, 58002 (2019).
- [28] H. Zhang, X. Liu, Y. Bao, Y. Zhang, and J. Zhao, *Symmetry* **14**, 965 (2022).
- [29] E. Rivet, A. Brandstötter, K. G. Makris, H. Lissek, S. Rotter, and R. Fleury, *Nat. Phys.* **14**, 942 (2018).
- [30] H. Zhang, Y. Zhang, X. Liu, Y. Bao, and J. Zhao, *AIP Adv.* **12**, 065217 (2022).
- [31] C. E. Rüter, K. G. Makris, R. El-Ganainy, D. N. Christodoulides, M. Segev, and D. Kip, *Nat. Phys.* **6**, 192 (2010).
- [32] Z. Lin, H. Ramezani, T. Eichelkraut, T. Kottos, H. Cao, and D. N. Christodoulides, *Phys. Rev. Lett.* **106**, 213901 (2011).
- [33] L. Feng, Y. Xu, W. S. Fegadolli, M. Lu, J. E. Oliveira, V. R. Almeida, Y. Chen, and A. Scherer, *Nat. Mater.* **12**, 108 (2013).
- [34] R. Fleury, D. L. Sounas, and A. Alù, *Phys. Rev. Lett.* **113**, 023903 (2014).
- [35] Y. Liu, T. Hao, W. Li, J. Capmany, N. Zhu, and M. Li, *Light Sci. Appl.* **7**, 38 (2018).
- [36] Ş. K. Özdemir, S. Rotter, F. Nori, and L. Yang, *Nat. Mater.* **18**, 783 (2019).
- [37] H. Li, M. Rosendo-López, Y. Zhu, X. Fan, D. Torrent, B. Liang, J. Cheng, and J. Christensen, *Research* **2019**, 8345683 (2019).
- [38] J. Lan, X. Zhang, L. Wang, Y. Lai, and X. Liu, *Sci. Rep.* **10**, 10794 (2020).
- [39] See Supplemental Material at <http://link.aps.org/supplemental/10.1103/PhysRevB.106.094101> for details of derivation of formula, accessing the EPs with $\rho < 1$ and $\kappa = 1$, pressure distribution in-between the slab, non-Hermitian impurity-shielding effect, and frequency influences on the \mathcal{PT} -symmetric system.
- [40] H. Wu, X. Yang, D. Deng, and H. Liu, *Phys. Rev. A* **100**, 033832 (2019).
- [41] L. Zheng, Y. Wu, X. Ni, Z. Chen, M. Lu, and Y. Chen, *Appl. Phys. Lett.* **104**, 161904 (2014).
- [42] Z. Hou, H. Ni, and B. Assouar, *Phys. Rev. Applied* **10**, 044071 (2018).
- [43] Q. Wu, Y. Chen, and G. Huang, *J. Acoust. Soc. Am.* **146**, 850 (2019).
- [44] M. Farhat, P.-Y. Chen, S. Guenneau, and Y. Wu, *Phys. Rev. B* **103**, 134101 (2021).